Geophysical Research Letters

RESEARCH LETTER
10.1029/2025GL116731

Strong ENSO Forcing of Wet Season Rainfall Extremes in the Eastern Amazon

L. Guimarães-Pereira[1], A. C. Barbosa[1], D. W. Stahle[2], M. C. A. Torbenson[3], D. Granato-Souza[4], C. L. Farrapo[1], E. Gloor[5], R. Brienen[5], and A. Boom[6]

[1]Departamento de Engenharia Florestal, Universidade Federal de Lavras, Lavras, Brazil, [2]Department of Geosciences, University of Arkansas, Fayetteville, AR, USA, [3]Department of Geography, Johannes Gutenberg University, Mainz, Germany, [4]Natural Resources and Environmental Sciences, Alabama A&M University, Huntsville, AL, USA, [5]School of Geography, University of Leeds, West Yorkshire, UK, [6]School of Geography, Geology & the Environment, University of Leicester, Leicester, UK

Abstract Recent years have seen strong droughts and floods in the Amazon basin, the largest center of atmospheric convection on land. To assess to what degree these events are extreme in a historical perspective requires accurate and long-term climate data, which are generally lacking for this part of the world. Here, we developed a 131-year oxygen isotope chronology from exactly dated tree rings of *Cedrela odorata* from the eastern Amazon Basin. The chronology (1885–2016) correlates strongly with observed wet-season rainfall totals ($r = -0.71$, 1951–2016) and stream discharge over the eastern equatorial Amazon. In contrast to oxygen isotope chronologies further inland that record basin-wide rainfall, our new record provides a good rainfall proxy for the eastern Amazon basin alone and shows that extreme precipitation events are also driven by ENSO.

Plain Language Summary The Amazon Basin is a crucial ecosystem for global biodiversity and climate, yet recent extreme droughts and floods raise concerns about the hydrological cycle over the Basin. Understanding these climate extremes is limited by the lack of long instrumental observations before 1950. Tree-ring data can provide a valuable proxy for historical climate variability. Oxygen isotope measurements from tree rings of *Cedrela odorata* were used here to reconstruct wet season rainfall over the eastern Amazon from 1885 to 2016. The reconstruction is very highly correlated with regional rainfall and river discharge, and with indices of the El Niño/Southern Oscillation. The lowest rainfall total observed in the instrumental measurements and in the reconstruction occurred in 1983, during one of the strongest El Niño events in recorded history. The new reconstruction provides a valuable addition to the hydroclimatic record for the late 19th and early 20th century in a data sparse region of the eastern Amazon.

Key Points:

- Oxygen isotopes in *Cedrela odorata* tree rings correlated with wet season rainfall and river discharge in the eastern equatorial Amazon
- The isotope proxy is used to reconstruct wet season rainfall totals from 1885 to 2016
- The 1983 El Niño event was associated with the largest rainfall deficit in eastern Amazonia in both instrumental and reconstructed records

Supporting Information:

Supporting Information may be found in the online version of this article.

Correspondence to:

L. Guimarães-Pereira and A. C. Barbosa, lucasgpereira.florestal@gmail.com.br; anabarbosa@ufla.br

Citation:

Guimarães-Pereira, L., Barbosa, A. C., Stahle, D. W., Torbenson, M. C. A., Granato-Souza, D., Farrapo, C. L., et al. (2025). Strong ENSO forcing of wet season rainfall extremes in the eastern Amazon. *Geophysical Research Letters*, *52*, e2025GL116731. https://doi.org/10.1029/2025GL116731

Received 28 APR 2025
Accepted 17 JUL 2025

Author Contributions:

Conceptualization: L. Guimarães-Pereira, A. C. Barbosa, D. W. Stahle, R. Brienen
Data curation: L. Guimarães-Pereira, D. W. Stahle, D. Granato-Souza
Formal analysis: L. Guimarães-Pereira, M. C. A. Torbenson, R. Brienen, A. Boom
Funding acquisition: A. C. Barbosa, D. W. Stahle, E. Gloor, R. Brienen
Investigation: L. Guimarães-Pereira, A. C. Barbosa, D. W. Stahle, C. L. Farrapo, E. Gloor
Methodology: L. Guimarães-Pereira, A. C. Barbosa, D. W. Stahle, M. C. A. Torbenson, D. Granato-Souza, C. L. Farrapo, R. Brienen, A. Boom

1. Introduction

The Amazon River basin is the largest continental center of atmospheric convection with the greatest river discharge to the ocean and highest biodiversity on Earth (Nobre, 2014; Zapata-Ríos et al., 2021). Intensification of the hydrological cycle over the Amazon has been observed during the last 35-year, including an increase in the frequency of extreme droughts and floods that were previously considered once-in-a-century events (Cintra et al., 2025; Espinoza et al., 2024; Gloor et al., 2013; Jiménez-Muñoz et al., 2016; Marengo & Espinoza, 2016). This trend in extremes may be linked to the complex interaction of deforestation in the drainage basin (Callède et al., 2004; Leite-Filho et al., 2020; Spracklen & Garcia-Carreras, 2015; Sternberg, 1987; Xu et al., 2022), natural variability of the coupled climate system (Barichivich et al., 2018; McGregor et al., 2014), and anthropogenic climate change (B. I. Cook et al., 2020; Ritchie et al., 2022).

Rainfall over the eastern Amazon Basin is strongly linked to the Walker Circulation and El Niño–Southern Oscillation (ENSO) (Cai et al., 2020). During El Niño years, anomalous tropospheric subsidence occurs over the northeastern Basin, while La Niña years bring the opposite pattern. Severe Amazon droughts are often associated with El Niño, whereas floods typically occur during La Niña. The 2023 drought, during an El Niño, was the driest on record, with the lowest Rio Negro levels at Manaus since 1901 (Espinoza et al., 2024). However, the instrumental record for Amazon precipitation and discharge extremes is limited. Few meteorological or discharge data exist before 1950, and many records are incomplete or affected by inhomogeneities (Granato-Souza et al., 2020). Therefore, longer and more continuous proxy records are essential to understanding long-term changes in the Amazon hydrological cycle.

Supervision: A. C. Barbosa, D. W. Stahle
Visualization: L. Guimarães-Pereira
Writing – original draft: L. Guimarães-Pereira, A. C. Barbosa, D. W. Stahle
Writing – review & editing: L. Guimarães-Pereira, A. C. Barbosa, D. W. Stahle, M. C. A. Torbenson, D. Granato-Souza, C. L. Farrapo, E. Gloor, R. Brienen, A. Boom

Ring-width chronologies of *C. odorata* from Rio Paru in the eastern Amazon have been used to reconstruct wet season rainfall totals and to examine the influence of ENSO in the eastern equatorial Amazon (Granato-Souza et al., 2018, 2020). These precipitation reconstructions have been substantiated with historical descriptions of drought and floods along the Amazon River during the 19th century (Granato-Souza & Stahle, 2023), suggesting that recent low river levels may have been equaled during the "Forgotten Drought" of 1865. While these historical records are useful, they are descriptive in nature and lack continuity. A powerful supplement to these records are oxygen isotopes derived from *C. odorata* tree rings in the Amazon which have been proven to be excellent proxies for precipitation (Baker et al., 2022; Brienen et al., 2012), surpassing the rainfall sensitivity of the ring-width chronologies.

Expanding on this potential, recent tree-ring oxygen isotope ($\delta^{18}O_{tr}$) records have been shown to capture precipitation signals across tropical South America (Alvarez et al., 2024; Cintra et al., 2025; Rodriguez-Caton et al., 2024). In the Amazon it has been shown that $\delta^{18}O_{tr}$ variation in tree rings of the genus *Cedrela* primarily reflect processes that influence the oxygen isotopic composition of precipitation ($\delta^{18}O_p$) (Baker et al., 2015, 2022; Brienen et al., 2012; Ortega-Rodriguez et al., 2023; Vargas et al., 2022). Two primary mechanisms are identified: the local amount effect and the continental effect (Baker et al., 2016; Dansgaard, 1964). Every precipitation event leads to depletion of heavy isotope in remaining water vapor in air. However, it has been found that locally, the degree of isotopic depletion varies with the precipitation intensity (Lee & Fung, 2008). For very intense precipitation events the $\delta^{18}O_p$ per precipitation amount is lower than for low intensity precipitation (e.g. drizzle, Dansgaard, 1964; Risi et al., 2008). In contrast, the continental effect refers to the gradual depletion of heavy isotopes in water vapor as air masses move inland. This happens because successive precipitation events preferentially remove heavier isotopes, leaving the remaining moisture that is transported further inland increasingly depleted in $\delta^{18}O$ (Vuille et al., 2003). Additionally, other factors can affect the $\delta^{18}O_{tr}$ signal, such as water recycling through tree evapotranspiration (Salati et al., 1979) and isotopic enrichment of leaf water due to evaporation (Barbour, 2007; Barbour et al., 2002).

For this study, we measured oxygen isotope ratios in exactly dated annual growth rings of *C. odorata* collected near the Rio Paru, in the eastern Amazon, to develop an improved reconstruction of wet season rainfall totals, to document the strength and consistency of ENSO forcing over the past 131-year, and to provide a longer paleoclimate perspective on the recent intensification of hydroclimatic extremes over the eastern equatorial Amazon.

2. Materials and Methods

2.1. Specie and Study Site

Samples of *Cedrela odorata* were collected in a legal logging concession near the Rio Paru, northeastern Brazilian Amazon (0.97°S, 53.32°W; Figure 1a), within the Paru State Forest, Pará. Annual precipitation ranged from 1,440 to 2,700 mm (1981–2016). The wet season extends from late January to June, with less than 60 mm per month during the dry season. Mean annual temperature varies little, between 26 and 27°C (Figure S1 in Supporting Information S1). *C. odorata* shows cambial dormancy in the dry season when leafless, with growth concentrated in the wet season (Dünisch et al., 2003). This aligns with local growth–climate relationships (Granata-Souza et al., 2018).

The Paru State Forest is situated at 400 to 800 masl and is mostly covered (95%) with tropical rainforest. Cross sections were cut from 45 legally harvested *C. odorata* trees (Rio Paru Site A: RPA), then dried, polished, and dendrochronologically dated. The ring-width chronology spans 1786–2016 (RBAR = 0.246), and numerical ring-width and chronology data are available from the International Tree-Ring Data set Bank at the NOAA National Center for Environmental Information (collection number BRA001; Granato-Souza et al., 2018).

2.2. Isotope Extraction and Chronology Development

Seven previously dated *Cedrela* specimens were selected for isotopic measurements based on their age, presence of pith, and the width and clarity of the dated annual growth rings. The cellulose extraction process followed the methodology described by Wieloch et al. (2011) and Kagawa et al. (2015) (see Text S1 in Supporting Information S1). The mean $\delta^{18}O_{tr}$ chronology was calculated as the average of the individual isotope series for each year with sample sizes (Figure S3 in Supporting Information S1). The agreement among the individual isotope

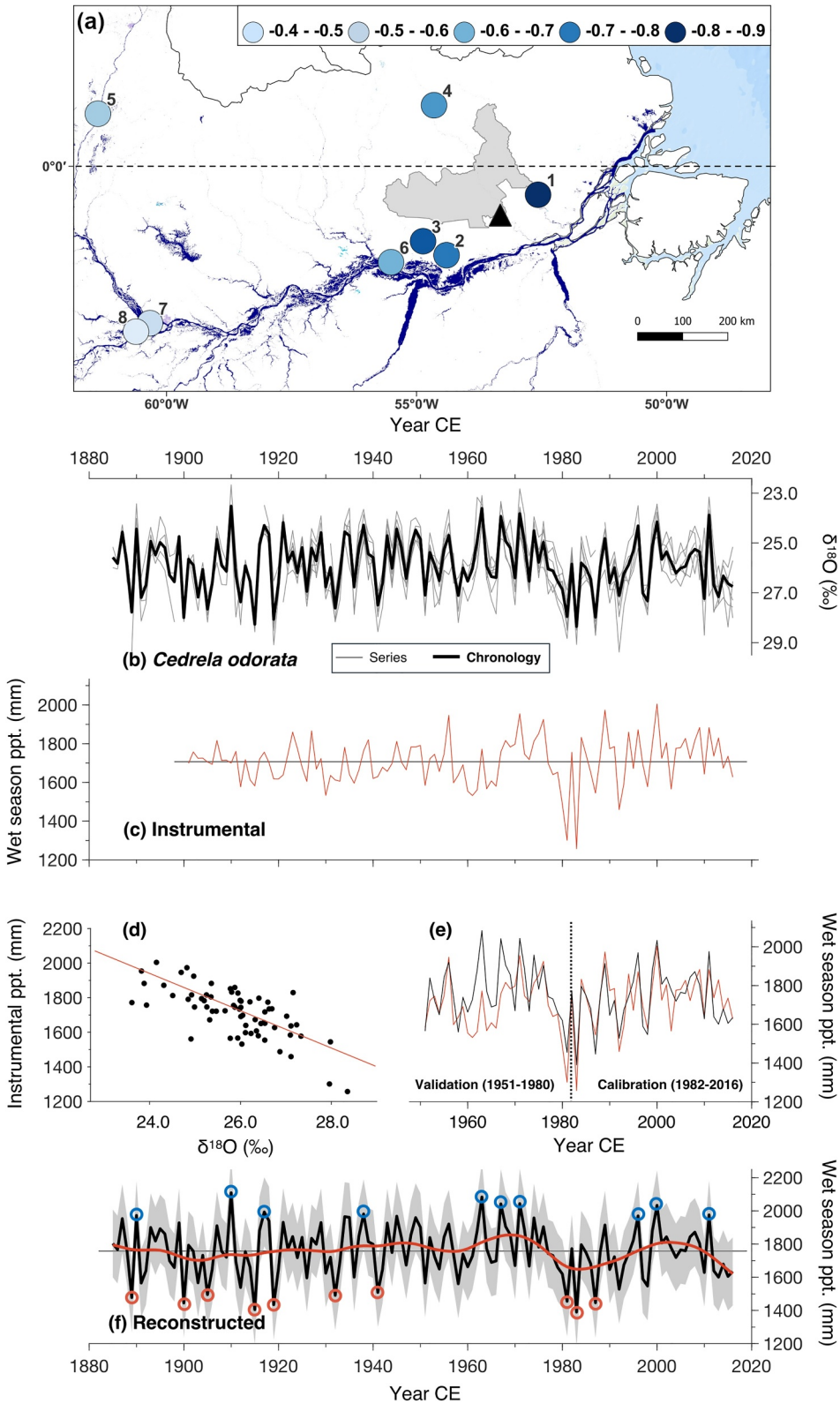

Figure 1.

series was assessed using the mean inter-series correlation (RBAR; E. R. Cook & Pederson, 2010) and Expressed Population Signal (EPS, Wigley et al., 1984).

2.3. Climate Data, Reconstruction, and Analyses

Pearson's and partial correlation analyses were conducted to compare the $\delta^{18}O_{tr}$ chronology with monthly climate data and identify which climate variables and seasons were most closely related to $\delta^{18}O_{tr}$. Precipitation totals (PPT) and mean temperature data were extracted from the CRU TS v4.07 data set (Harris et al., 2020) using the KNMI Climate Explorer (Trouet & Oldenborgh, 2013, https://climexp.knmi.nl/) for a grid box in northeastern Amazon (Figure S2 in Supporting Information S1, 1901 to 2022), selecting the region with strongest correlation to $\delta^{18}O_{tr.}$ Due to limited local station data, vapor pressure deficit (VPD) was calculated using actual vapor pressure and temperature data from CRU TS v4.07. River discharge and stream level data were sourced from the HydroWeb website of the Brazilian National System of Hydric Resources Information (SNIRH, www.snirh.gov.br).

Based on correlation analyses with monthly climate data, we used bivariate regression to calibrate the $\delta^{18}O_{tr}$ chronology with wet season (January–June) precipitation and reconstructed rainfall from 1885 to 2016. To assess uncertainty, we computed semi-parametric 95% prediction intervals (E. R. Cook et al., 2013) using point-by-point regression (E. R. Cook et al., 1999), least squares theory (Olive, 2007; Seber & Lee, 2003), and maximum entropy bootstrap (Vinod, 2006). Reconstruction reliability was evaluated for the independent validation period (1951–1981) using squared Pearson correlation (R^2), average reduction error (RE), and average coefficient of efficiency (CE) statistics (E. R. Cook et al., 1999), when instrumental precipitation data were sufficiently replicated.

The precipitation reconstruction was correlated with gridded sea level pressure (SLP; ERA5, Hersbach et al., 2020), sea surface temperature (SST; HadlSST1, Rayner et al., 2003), and the Southern Oscillation Index (SOI; CRU; Allan et al., 1991). The Multivariate ENSO Index (MEI; Wolter & Timlin, 2011) was used to assess the ENSO signal in reconstructed precipitation for the eastern Amazon. We also performed a spatial correlation analysis to identify a broader Pan-American climate signal captured by the $\delta^{18}O_{tr}$ record. Singular Spectrum Analysis (SSA; Ghil et al., 2002; St. George & Ault, 2011) identified quasi-periodic components in the instrumental and reconstructed rainfall data. Cross-spectral coherence (Percival & Constantine, 2006) measured frequency domain agreement between ENSO and instrumental and reconstructed rainfall over the eastern Amazon using the December–April Nino 3.4 SST Index (Rayner et al., 2003).

3. Results

3.1. Hydroclimatic Signals in the $\delta^{18}O_{tr}$ Chronology

The oxygen isotope records are highly correlated among trees (Figure 1b and Figure S3 in Supporting Information S1), significantly more so than the correlation between ring width time series from the same seven *Cedrela* trees at the Rio Paru site (RBAR = 0.74 and 0.33, respectively). The mean $\delta^{18}O_{tr}$ chronology is significantly correlated with January–June precipitation totals in the eastern equatorial Amazon ($r = -0.62$, $p < 0.0001$; 1901–2016; Figure S2 and Table S1 in Supporting Information S1). However, precipitation data from the early 20th century lack stations near the study site (Figure S2 in Supporting Information S1), leading to inhomogeneity in the instrumental January–June precipitation time series variance, especially before 1960 (Figure 1c). Correlation between the $\delta^{18}O_{tr}$ chronology and precipitation improves post-1950 ($r = -0.71$, $p < 0.0001$; 1951–2016),

Figure 1. (a) The $\delta^{18}O_{tr}$ chronology (black triangle) is located within the forest concession area of the Paru State Forest (gray shade), 100 km north of the Amazon River. Streamflow data (circles) were selected from stations with records from 1980 to 2012: 1. Jari River, 2. Maicuru River, 3. Curuá River, 4. Paru River, 5. Branco River, 6. Amazon River (Óbidos), 7. Negro River (Manaus)*, and 8. Solimões River (Manacapuru). Colors indicate Pearson correlations between $\delta^{18}O_{tr}$ and January–June discharge, all statistically significant. *Data for the Negro River reflect water levels only. (b) The $\delta^{18}O_{tr}$ series for seven *Cedrela odorata* trees from the Rio Paru (gray) and their mean (black) from 1885 to 2016 (sample size: 2–7 series/year, Figure S3 in Supporting Information S1). Note the inverted *x*-axis. (c) January–June regional instrumental precipitation extracted from CRU TS v4.07 (box area in Figure S2 in Supporting Information S1) for 1901–2016 in the eastern equatorial Amazon, including the Rio Paru sampling site. (d) Scatterplot comparing $\delta^{18}O_{tr}$ with regional instrumental January–June precipitation totals, 1951–2016. (e) Reconstructed (black) versus regional instrumental (red) January–June precipitation totals, 1951–2016 (validation 1951–1981, calibration 1982–2016). (f) Reconstructed January–June precipitation for eastern Amazon (1885–2016) with 95% prediction intervals (gray) and 20-year smoothing (red). Red circles = 10 driest years: 1889, 1900, 1905, 1915, 1919, 1932, 1941, 1981, 1983, 1987; blue circles = 10 wettest years: 1890, 1910, 1917, 1938, 1963, 1971, 1996, 2000, 2011.

coinciding with increased numbers and better spatial distribution of rainfall recording stations (Figure S2 in Supporting Information S1). Relationships with mean wet season surface air temperature and VPD are much weaker ($r = 0.47$ ($p < 0.001$) and $r = 0.40$ ($p < 0.01$), respectively; 1951–2016, Table S1 in Supporting Information S1), compared to the hydroclimate correlations. To assess the independent effect of precipitation on $\delta^{18}O_{tr}$, we conducted partial correlation analyses controlling for temperature and VPD. Results indicate a robust correlation with precipitation ($r = -0.60$), confirming it as the primary climatic driver. In contrast, correlations with temperature ($r = 0.18$) and VPD ($r = 0.06$) were weak, suggesting limited influence on $\delta^{18}O_{tr}$ variability.

Additionally, the $\delta^{18}O_{tr}$ chronology is highly correlated with river discharge measured on several tributaries to the eastern Amazon, including the Rio Jari ($r = -0.87$; $p < 0.0001$; 1970–2013) and the Rio Maicuru ($r = -0.84$; $p < 0.0001$; 1970–2013) (Figure 1a). The $\delta^{18}O_{tr}$ chronology is also significantly correlated with total annual discharge of the Amazon River measured at Óbidos ($r = -0.53$, $p < 0.01$; 1968–2014), despite the vast drainage basin area upstream of the gauge and the considerable distance to the isotope study site.

3.2. Reconstructed Precipitation, 1885–2016

The $\delta^{18}O_{tr}$ series explains nearly two thirds of the variance in the instrumental precipitation data during the 1982–2016 calibration period ($R^2_{adj} = 0.62$; Figure 1e). The derived reconstruction is correlated with January–June precipitation during the independent validation period from 1951 to 1981 ($r = 0.51$). The reduction of error and coefficient of efficiency statistics computed on this validation interval are also both positive (RE = 0.27; CE = 0.21).

The precipitation reconstruction is plotted from 1885 to 2016 along with the 95% prediction error intervals and a 20-year smoothing (Figure 1f). The reconstruction is 131-year long and only extends the regional CRU instrumental precipitation data by 16 years. However, in this data poor region of the Amazon the $\delta^{18}O_{tr}$ reconstructed precipitation data are a useful addition for the entire pre-calibration interval prior to 1982. The driest year in both the instrumental (Figure 1b, 1901–2016) and reconstructed records (Figure 1f, 1885–2016) occurred in 1983 during one of the strongest El Niño events in recorded history (Quiroz, 1983), followed by the drought of 1981 that was nearly as severe as 1983 (Figure 1e).

The instrumental and reconstructed precipitation time series both record a decade-long dry period from 1978 to 1987. The period from 1897 to 1906 was the only other decade-long interval in the reconstruction to approach the dryness observed and reconstructed in the late 1970s and 80s (Figure 1f). The reconstruction indicates a wet interval from 1962 to 1976 that is only partially evident in the instrumental precipitation data (Figure 1f). This difference and the decline in average instrumental precipitation that begins in 1967 and extends back to the beginning of the observations in 1901 (Figure 1c) may both be related to limited nearby station observations available in the CRU data set (e.g., Granato-Souza et al., 2020; Figure S2 in Supporting Information S1). Inhomogeneity in the instrumental observations is also indicated by the difference in correlation with the reconstructed rainfall series before and after 1980 ($r = 0.56$, 1901–1980; $r = 0.81$, 1981–2016).

3.3. Large-Scale Climate Controls on Precipitation Variation

ENSO forcing of rainfall in the eastern Amazon is evident from the correlations of reconstructed and instrumental precipitation totals with gridded SLP and SST data from 1950 to 2015 (Figures 2a–2e, Table S2 in Supporting Information S1). These correlations confirm that cool SSTs in Nino3.4 region, which are associated with La Niña conditions, are linked to heavy rainfall, while warm SSTs during El Niño conditions are associated with a drought in the eastern Amazon. This ENSO forcing of wet season rainfall in the eastern Amazon is also illustrated by correlation analyses with the December–April SOI (Table S2 in Supporting Information S1). The SOI shows a strong covariation with the reconstructed precipitation time series both before and after 1950 ($r = 0.68$, 1901–1950 vs. 0.70 for 1951–2015), but correlations between SOI and instrumental precipitation decrease strongly for the period before 1950 when using instrumental January–June precipitation ($r = 0.43$, 1901–1950 vs. 0.64 for 1951–2015). The weakening SOI signal in the instrumental precipitation data before 1950 likely reflects changes in the stations available for the regional average over the northeast Amazon. In fact, the instrumental precipitation data are based on just three stations before 1911, Manaus, Georgetown (Guyana) and Cultuurtuin (Paramaribo, Suriname), which are all located at least 770 km from the study area, and the number of stations exceeds 10 only after 1927 (Figure S2 in Supporting Information S1). This huge change in the spatial aggregation

10.1029/2025GL116731

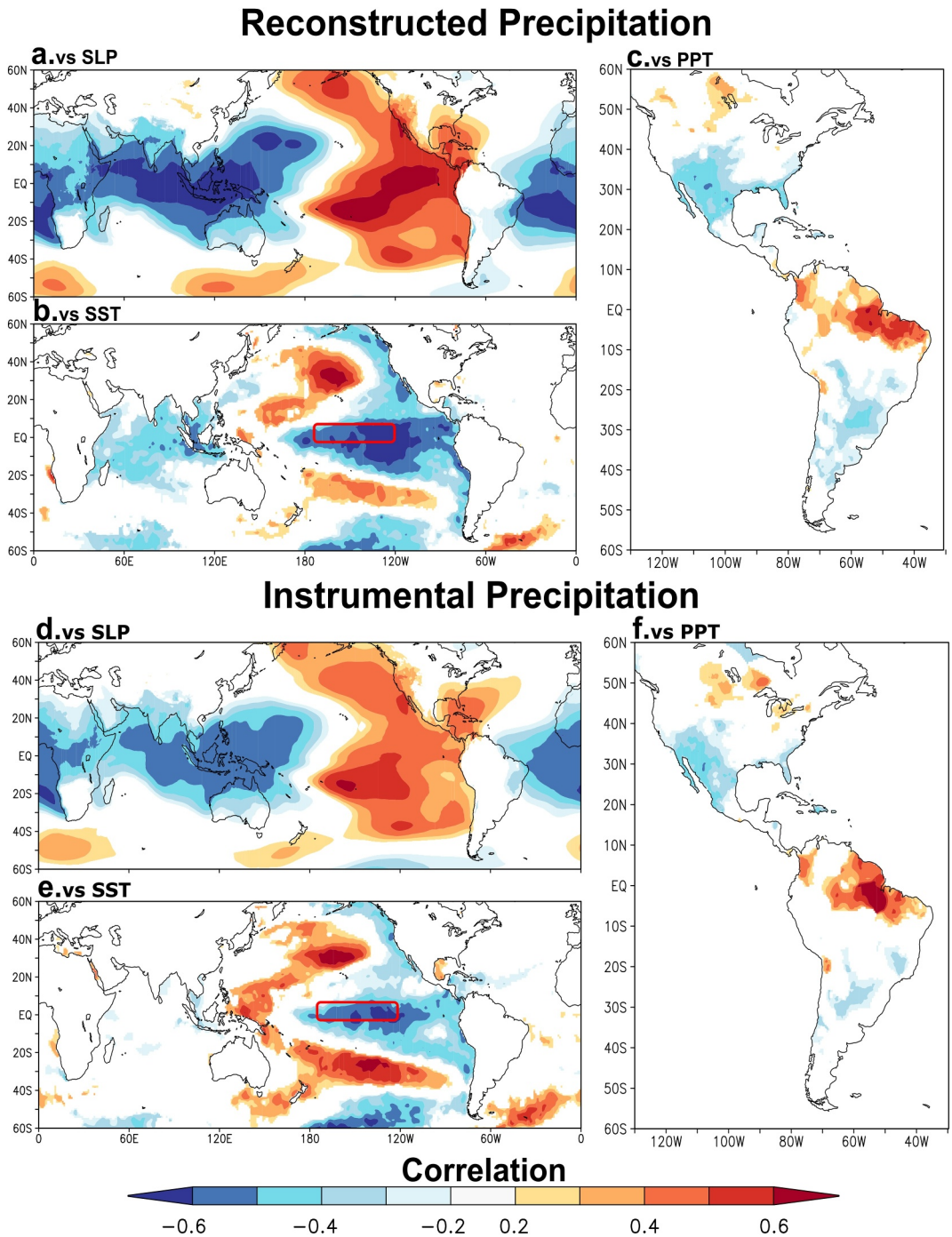

Figure 2. Correlations of large-scale climate signal in reconstructed and instrumental precipitation from the eastern Amazon. Reconstructed wet season precipitation totals (January–June) from the eastern Amazon are correlated with gridded ERA5 SLP (a) and HadlSST1 (b) for December–April from 1950 to 2015, and with CRU TS v4.07 November–May precipitation totals (PPT) (c) over the Americas, also from 1950 to 2015 ($p < 0.10$ for all correlations, computed with the *KNMI Climate Explorer*). (e–f) Same as (a–c) for instrumental precipitation. The NINO3.4 region is indicated (red box).

of the instrumental observations underscores the value of the new $\delta^{18}O_{tr}$-based precipitation reconstruction for analyses of climate variability and climate forcing in the eastern Amazon during the past 131-year.

Reconstructed and instrumental wet season precipitation totals at Paru are positively and significantly correlated with precipitation over a large sector of the eastern Amazon and northeast Brazil (Figure 2). They are also

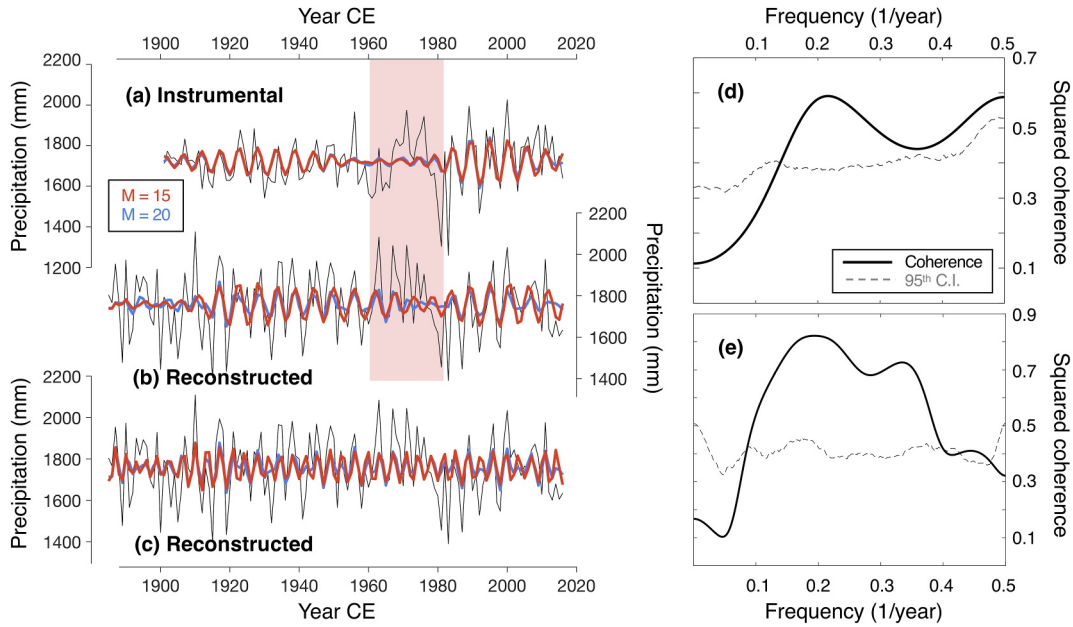

Figure 3. Periodicities and coherence patterns in $\delta^{18}O_{tr}$-based precipitation estimates, instrumental rainfall, and climate indices. (a) Reconstructed components (RCs) from singular spectrum analysis of instrumental rainfall highlight RC3 and RC4 (window lengths of 15 and 20 years), showing a 5.5-year periodicity and accounting for 18.8% and 16.1% of total variance, respectively. (b) This 5.5-year signal is also present in $\delta^{18}O_{tr}$-estimated rainfall for lag windows of 15 (red; RC1, RC3, RC4) and 20 (blue; RC3, RC4) years, explaining 27.9% and 15.9% of variance, respectively. (c) A 3.5-year periodicity is seen in RC2 ($M = 15$) and RC1/RC2 ($M = 20$), representing 10.4% and 17.6% of total variance. The instrumental RCs (a) show reduced amplitude from ~1965 to 1980, mirrored in the $\delta^{18}O_{tr}$ series (b, c). (d) Squared coherency between $\delta^{18}O_{tr}$-based precipitation and instrumental rainfall (1951–2016), with dashed lines marking $p \leq 0.05$. (e) As in (d) but comparing with the Niño3.4 SST index (Dec–Apr 1885–2016).

negatively correlated with total precipitation over subtropical North and South America (Figure 2). For these comparisons the gridded CRU precipitation data were averaged for a November–May season because the simultaneous hemispheric-wide correlations are maximized during this season (Stahle et al., 2020). For wet season rainfall in the eastern Amazon, both instrumental and reconstructed, the North American precipitation correlations are strongest from December–April and the South American correlations are highest during the prior September–November period (not shown). The November–May interval appears to best integrate these seasonal differences during the 1950–2015 period. Figure 2 indicates that the interannual variability of wet season rainfall in the eastern Amazon is dominated by ENSO with little evidence of tropical Atlantic forcing. However, a marginally significant correlation with south tropical Atlantic SSTs can be observed when the influence of ENSO forcing is removed from the eastern Amazon rainfall series (i.e., correlating the residuals from a regression of the NINO 3.4 SST Index on eastern Amazon rainfall with gridded SSTs, 1950–2015, Figure S4 in Supporting Information S1).

The reconstruction records the dominant frequency components observed in the short instrumental precipitation data, which seem to originate from ENSO forcing. SSA indicates that the reconstruction has two strong quasi-periodicities at periods of 3.5- and 5.5-year (Figures 3a and 3b). These reconstructed components (RCs) together represent some 33%–38% of the reconstructed precipitation variance in the 1885–2016 period (depending on the lag window length, Figures 3a and 3b). Instrumental wet season precipitation also includes a strong 5.5-year periodicity (1951–2016; Figure 3c), and increased variance has been identified around these frequencies in indices of ENSO (e.g., Bruun et al., 2017; Gehne et al., 2014). Note also that the amplitude of the 5.5-year quasi-periodicity is attenuated in both the reconstructed and instrumental rainfall series during the period from ca 1965–1980 (Figures 3a and 3c). The reconstruction is coherent with instrumental rainfall at frequencies from 2- to 10-year (1950–2016; Figure 3d). The reconstruction also displays strong coherence with the Nino 3.4 SST Index at frequencies from approximately 3- to 10-year (1885–2016; Figure 3e and Table S2 in Supporting Information S1).

4. Discussion and Conclusions

We demonstrate that the *C. odorata* $\delta^{18}O_{tr}$ chronology from the Rio Paru provides a new proxy for rainfall over the eastern equatorial Amazon that is more sensitive compared to ring-width data from the same trees (Granato-Souza et al., 2018). The $\delta^{18}O_{tr}$-based precipitation reconstruction presented here explains 62% of the variance in the instrumental rainfall data during the period from 1982 to 2016. The reconstruction reveals an increase in low-frequency variability after 1959 with a relatively wet interval from 1960 to 1977, followed by a drier interval from 1978 to 1995. Extremely wet or dry years appear to have decreased in the eastern Amazon study area after 2000, in both the instrumental and reconstructed rainfall data (Figures 2a and 2e). No recent events exceeded the drought of 1983 or the wetness in 2000.

The large-scale ocean-atmospheric dynamics in the precipitation reconstruction are strongly associated with ENSO, which drives the interannual variability of rainfall in this region (Cai et al., 2020; Ronchail et al., 2002). The 10 driest and 10 wettest years in the reconstruction usually occurred during El Niño and La Niña conditions, respectively. However, ENSO does not account for all rainfall extremes in the eastern Amazon, as the severe deficits in wet season precipitation totals in 1981 and 1983 demonstrate. The El Niño event of 1983 was one of the strongest in recorded history and resulted in the lowest rainfall totals in both the 116-year instrumental and 131-year reconstructed series. Wet season rainfall in 1981 was almost as low but occurred under neutral to weak El Niño conditions. The extreme rainfall deficits of 1981 and 1983 skew the instrumental rainfall distribution for the study area, standing out as the years with the most pronounced anomalies in the entire data set.

The $\delta^{18}O_{tr}$-based precipitation reconstruction also captures earlier hydroclimatic extremes not clearly evident in instrumental records (Figure 1c) or Rio Negro discharge data (not shown). Notably, the wettest year (1910) and second driest (1915) align with strong La Niña and El Niño events, respectively, as shown by the extended MEI. These patterns highlight the reconstruction's ability to resolve ENSO-related variability in the eastern Amazon during periods of limited observational data. The isotope-based record validates these extremes and places them within a longer-term historical context extending back to the late 19th century.

The ENSO signal is strongest from December to February in the reconstructed precipitation series which likely reflects the seasonal peak in ENSO when the tropical Pacific has the strongest effect on global climate (E. R. Cook & Cane, 2024). ENSO forcing of the reconstruction is further highlighted by the significant anti-correlation with precipitation over subtropical North and South America. This Pan American precipitation pattern was identified in composite analyses of ring-width-estimated extremes from the Rio Paru collection site dating back to 1759 (Stahle et al., 2020). However, the inter-hemispheric signal is stronger and has a greater temporal stability in the shorter $\delta^{18}O_{tr}$-based precipitation reconstruction. When compared to an ENSO reconstruction from the US Southwest, based only on tree-ring widths chronologies that display temporally stable MEI signals (Torbenson et al., 2019), the wettest years and driest years correspond to positive and negative MEI indices respectively (Figure S5a in Supporting Information S1). Similarly, when the opposite is tested, all 10 La Niña years and seven of 10 El Niño years recorded in the US Southwest correspond to the expected sign of departures from the mean for the eastern Amazon rainfall reconstruction (Figure S5b in Supporting Information S1). This agreement with known ENSO-related precipitation anomalies in the US Southwest provides an independent validation of the $\delta^{18}O_{tr}$-based precipitation reconstruction, highlighting its consistency with large-scale climate teleconnections and reinforcing the reliability of the signal captured in the eastern Amazon.

Oxygen isotopes in tree rings have been correlated with river discharge in previous studies (e.g., Baker et al., 2022; Brienen et al., 2012). The available instrumental river discharge records for the eastern Amazon are short but several are highly correlated with the $\delta^{18}O_{tr}$-based precipitation reconstruction of wet season (e.g., $r = 0.87$ for the nearby Rio Jari; 1970–2014). These river flow correlations are as high or higher than the correlations between the instrumental and reconstructed rainfall series. The strong discharge correlations may reflect the basin-scale integration of precipitation by streamflow and indicate real potential for skillful reconstructions of discharge in important tributaries of the Amazon River based on $\delta^{18}O$ data from *C. odorata*.

The rainfall reconstruction from $\delta^{18}O_{tr}$ shows a modest correlation with basin-wide precipitation ($r = 0.27$, $p < 0.01$, 1901–2016; $r = 0.31$, $p < 0.01$, 1960–2016). This weak correlation contrasts with the strong relationships observed in the oxygen isotope chronologies of *Cedrela* sp. from Bolivia ($r = -0.73$, 1901–2014; Baker et al., 2022) and Rondônia ($r = -0.76$, 1960–2020; Ortega-Rodriguez et al., 2023), both located in the southwestern Amazon Basin. Variation in oxygen isotope composition in the south Amazon is the result of a

Rayleigh distillation process (Vuille et al., 2003). This Rayleigh process consists of the preferential removal of heavier water, $H_2{}^{18}O$, at each precipitation event during water vapor transport from the tropical north Atlantic to the southwestern parts of the Amazon basin. As a result, the remaining water vapor becomes more and more depleted leading to lower $\delta^{18}O_p$ at the end of the water vapor pathway. During years with high precipitation over the Amazon basin, more of the heavy water is lost resulting in lower $\delta^{18}O$ values in precipitation in the southwestern Amazon compared to dry years, explaining the strong correlation for these sites with basin-wide rainfall. In contrast, as our site is located just 300 km from the coast the chronology does not reflect basin-wide precipitation rainout processes. Instead, it reflects more local to regional amount effects as indicated by the limited extend of the spatial correlation (see Figure 2c) and consistent with tree ring oxygen isotopes studies from other coastal regions (Brienen et al., 2013). This local amount effect consists of the negative correlation between the precipitation rate, or intensity, and the resulting isotope signal in the precipitation (Dansgaard, 1964; Lee & Fung, 2008; Rozanski et al., 2013).

The strong correlations between our reconstruction and hydroclimatic variability over the eastern Amazon, particularly in contrast to the integrated effects of changes in the hydrological cycle across the basin, underscore the value of this new data set. The close estimation of the two most extreme instrumental precipitation deficits in 1981 and 1983, the coherence of the $\delta^{18}O_{tr}$-based precipitation reconstruction with instrumental rainfall and ENSO indices, and its ability to track amplitude modulation of instrumental rainfall data all validate this new wet season rainfall reconstruction. Although the current $\delta^{18}O_{tr}$-based reconstruction is only 131 years long, existing ring-width data from Rio Paru *C. odorata* dates back to 1759. Oxygen isotope analyses on older samples from Rio Paru are underway, holding promise for a longer paleoclimate perspective on precipitation and streamflow in this region of the Amazon, including large-magnitude droughts and floods documented with *C. odorata* ring widths and historical descriptions from the late 18th and 19th centuries. Such long-term reconstructions will help improve understanding of the current intensification of the Amazon hydrological cycle (Granato-Souza & Stahle, 2023).

Data Availability Statement

The isotope chronology data used in this study is available in the International Tree-Ring Data Bank at the NOAA National Center for Environmental and Paleoclimatology Information (Guimarães-Pereira et al., 2025).

Acknowledgments

We thank Sr. Evandro Dalmaso and Sra. Eliane Dalmaso of the CEMAL logging firm for access and logistical support. We appreciate the data provided by the Climatic Research Unit, University of East Anglia, and the use of the KNMI Climate Explorer. The data developed for this article have been contributed to the International Tree-Ring Data Bank at the NOAA Paleoclimatology Program (https://www.ncdc.noaa.gov/dataaccess/paleoclimatology-data). Funding provided by the U.S. National Science Foundation (AGS-2002374, AGS-2347844, AGS-2347845), LGP was supported by FAPEMIG (Grant APQ-01544-22). ACB acknowledges funding from CNPq (Grant PQ 313129/2022-3). RB, AB and MG acknowledge funding from NERC-UK (Grant NE/S008659/1).

References

Allan, R. J., Nicholls, N., Jones, P. D., & Butterworth, I. J. (1991). A further extension of the Tahiti-Darwin SOI, early SOI results and Darwin pressure. *Journal of Climate*, *4*(7), 743–749. https://doi.org/10.1175/1520-0442(1991)004<0743:afeott>2.0.co;2

Álvarez, C., Christie, D. A., González-Reyes, Á., Veblen, T. T., Helle, G., LeQuesne, C., et al. (2024). Hydroclimate variability in the Tropical Andes recorded by $\delta^{18}O$ isotopes from a new network of Polylepis Tarapacana tree-rings. *Global and Planetary Change*, *239*, 104503. https://doi.org/10.1016/j.gloplacha.2024.104503

Baker, J. C. A., Cintra, B. B. L., Gloor, M., Boom, A., Neill, D., Clerici, S., et al. (2022). The changing Amazon hydrological Cycle—Inferences from over 200 Years of tree-ring oxygen isotope data. *Journal of geophysical Research. Biogeosciences*, *127*(10), e2022JG006955. https://doi.org/10.1029/2022JG006955

Baker, J. C. A., Gloor, M., Spracklen, D. V., Arnold, S. R., Tindall, J. C., Clerici, S. J., et al. (2016). What drives interannual variation in tree ring Oxygen isotopes in the Amazon? *Geophysical Research Letters*, *43*(22). https://doi.org/10.1002/2016GL071507

Baker, J. C. A., Hunt, S. F. P., Clerici, S. J., Newton, R. J., Bottrell, S. H., Leng, M. J., et al. (2015). Oxygen isotopes in tree rings show good coherence between species and sites in Bolivia. *Global and Planetary Change*, *133*, 298–308. https://doi.org/10.1016/j.gloplacha.2015.09.008

Barbour, M. M. (2007). Stable oxygen isotope composition of plant tissue: A review. *Functional Plant Biology*, *34*(2), 83. https://doi.org/10.1071/FP06228

Barbour, M. M., Walcroft, A. S., & Farquhar, G. D. (2002). Seasonal variation in $\delta^{13}C$ and $\delta^{18}O$ of cellulose from growth rings of Pinus Radiata. *Plant, Cell and Environment*, *25*(11), 1483–1499. https://doi.org/10.1046/j.0016-8025.2002.00931.x

Barichivich, J., Gloor, E., Peylin, P., Brienen, R., Schongart, J., Espinoza, J. C., & Pattnayak, K. C. (2018). Recent intensification of Amazon flooding extremes driven by strengthened Walker circulation. *Science Advances*, *4*(9). https://doi.org/10.1126/sciadv.aat8785

Brienen, R. J. W., Helle, G., Pons, T. L., Guyot, J.-L., & Gloor, M. (2012). Oxygen isotopes in tree rings are a good proxy for Amazon precipitation and El Niño-Southern Oscillation variability. *Proceedings of the National Academy of Sciences*, *109*(42), 16957–16962. https://doi.org/10.1073/pnas.1205977109

Brienen, R. J. W., Hietz, P., Wanek, W., & Gloor, M. (2013). Oxygen isotopes in tree rings record variation in precipitation $\delta^{18}O$ and amount effects in the south of Mexico. *Journal of Geophysical Research: Biogeosciences*, *118*(4), 1604–1615. https://doi.org/10.1002/2013JG002304

Bruun, J. T., Allen, J. I., & Smyth, T. J. (2017). Heartbeat of the Southern Oscillation explains ENSO climatic resonances. *Journal of Geophysical Research: Oceans*, *122*(8), 6746–6772. https://doi.org/10.1002/2017JC012892

Cai, W., McPhaden, M. J., Grimm, A. M., Rodrigues, R. R., Taschetto, A. S., Garreaud, R. D., et al. (2020). Climate impacts of the El Niño–Southern oscillation on South America. *Nature Reviews Earth & Environment*, *1*(4), 215–231. https://doi.org/10.1038/s43017-020-0040-3

Callède, J., Guyot, J. L., Ronchail, J., L'Hôte, Y., Niel, H., & de Oliveira, E. (2004). Evolution du débit de l'Amazone à Óbidos de 1903 à 1999/Evolution of the River Amazon's discharge at Óbidos from 1903 to 1999. *Hydrological Sciences Journal*, *49*(1), 85–97. https://doi.org/10.1623/hysj.49.1.85.53992

Cintra, B. B. L., Gloor, E., Baker, J. C. A., Boom, A., Schöngart, J., Clerici, S., et al. (2025). Tree ring isotopes reveal an intensification of the hydrological cycle in the Amazon. *Communications Earth & Environment*, *6*(1), 453. https://doi.org/10.1038/s43247-025-02408-9

Cook, B. I., Mankin, J. S., Marvel, K., Williams, A. P., Smerdon, J. E., & Anchukaitis, K. J. (2020). Twenty-first century drought projections in the CMIP6 forcing scenarios. *Earth's Future*, *8*(6), e2019EF001461. https://doi.org/10.1029/2019EF001461

Cook, E. R., & Cane, M. A. (2024). Tree rings reveal ENSO in the last millennium. *Geophysical Research Letters*, *51*(19), e2024GL109759. https://doi.org/10.1029/2024GL109759

Cook, E. R., Meko, D. M., Stahle, D. W., & Cleaveland, M. K. (1999). Drought reconstructions for the continental United States. *Journal of Climate*, *12*(4), 1145–1162. https://doi.org/10.1175/1520-0442(1999)012<1145:DRFTCU>2.0.CO;2

Cook, E. R., Palmer, J. G., Ahmed, M., Woodhouse, C. A., Fenwick, P., Zafar, M. U., et al. (2013). Five centuries of upper Indus River flow from tree rings. *Journal Hydrology*, *486*, 365–375. https://doi.org/10.1016/j.jhydrol.2013.02.004

Cook, E. R., & Pederson, N. (2010). Uncertainty, emergence, and statistics in dendrochronology. In M. K. Hughes, T. W. Swetnam, & H. F. Diaz (Eds.), *Dendroclimatology* (Vol. 11, pp. 77–112). Springer. https://doi.org/10.1007/978-1-4020-5725-0_4

Dansgaard, W. (1964). Stable isotopes in precipitation. *Tellus*, *16*(4), 436–468. https://doi.org/10.1111/j.2153-3490.1964.tb00181.x

Dünisch, O., Montóia, V. R., & Bauch, J. (2003). Dendroecological investigations on Swietenia macrophylla king and Cedrela odorata L. (Meliaceae) in the central Amazon. *Trees*, *17*(3), 244–250. https://doi.org/10.1007/s00468-002-0230-2

Espinoza, J.-C., Jimenez, J. C., Marengo, J. A., Schongart, J., Ronchail, J., Lavado-Casimiro, W., & Ribeiro, J. V. M. (2024). The new record of drought and warmth in the Amazon in 2023 related to regional and global climatic features. *Scientific Reports*, *14*(1), 8107. https://doi.org/10.1038/s41598-024-58782-5

Gehne, M., Kleeman, R., & Trenberth, K. E. (2014). Irregularity and decadal variation in ENSO: A simplified model based on principal oscillation patterns. *Climate Dynamics*, *43*(12), 3327–3350. https://doi.org/10.1007/s00382-014-2108-6

Ghil, M., Allen, M. R., Dettinger, M. D., Ide, K., Kondrashov, D., Mann, M. E., et al. (2002). Advanced spectral methods for climatic time series. *Reviews of Geophysics*, *40*(1), 3-1-3–41. https://doi.org/10.1029/2000RG000092

Gloor, M., Brienen, R. J. W., Galbraith, D., Feldpausch, T. R., Schöngart, J., Guyot, J.-L., et al. (2013). Intensification of the Amazon hydrological cycle over the last two decades. *Geophysical Research Letters*, *40*(9), 1729–1733. https://doi.org/10.1002/grl.50377

Granato-Souza, D., & Stahle, D. W. (2023). Drought and flood extremes on the Amazon River and in northeast Brazil, 1790–1900. *Journal of Climate*, *36*(20), 7213–7229. https://doi.org/10.1175/JCLI-D-23-0146.1

Granato-Souza, D., Stahle, D. W., Barbosa, A. C., Feng, S., Torbenson, M. C. A., de Assis Pereira, G., et al. (2018). Tree rings and rainfall in the equatorial Amazon. *Climate Dynamics*, *52*(3–4), 1857–1869. https://doi.org/10.1007/s00382-018-4227-y

Granato-Souza, D., Stahle, D. W., Torbenson, M. C. A., Howard, I. M., Barbosa, A. C., Feng, S., et al. (2020). Multidecadal changes in wet season precipitation totals over the eastern Amazon. *Geophysical Research Letters*, *47*(8), e2020GL087478. https://doi.org/10.1029/2020GL087478

Guimarães-Pereira, L., Barbosa, A. C., Stahle, D. W., Torbenson, M. A. C., Granato-Souza, D., Farrapo, C. L., et al. (2025). NOAA/WDS paleoclimatology—Eastern Amazon tree ring oxygen stable isotopes and precipitation reconstruction 1885–2016 CE [Dataset]. *NOAA National Centers for Environmental Information*. https://doi.org/10.25921/PAXP-VA86

Harris, I., Osborn, T. J., Jones, P., & Lister, D. (2020). Version 4 of the CRU TS monthly high-resolution gridded multivariate climate dataset. *Scientific Data*, *7*(1), 109. https://doi.org/10.1038/s41597-020-0453-3

Hersbach, H., Bell, B., Berrisford, P., Hirahara, S., Horányi, A., Muñoz-Sabater, J., et al. (2020). The ERA5 global reanalysis. *Quarterly Journal of the Royal Meteorological Society*, *146*(730), 1999–2049. https://doi.org/10.1002/qj.3803

Jiménez-Muñoz, J. C., Mattar, C., Barichivich, J., Santamaría-Artigas, A., Takahashi, K., Malhi, Y., et al. (2016). Record-breaking warming and extreme drought in the Amazon rainforest during the course of El Niño 2015–2016. *Scientific Reports*, *6*(1). https://doi.org/10.1038/srep33130

Kagawa, A., Sano, M., Nakatsuka, T., Ikeda, T., & Kubo, S. (2015). An optimized method for stable isotope analysis of tree rings by extracting cellulose directly from cross-sectional laths. *Chemical Geology*, *393–394*, 16–25. https://doi.org/10.1016/j.chemgeo.2014.11.019

Lee, J. E., & Fung, I. (2008). "Amount effect" of water isotopes and quantitative analysis of post-condensation processes. Hydrological processes. *International Journal*, *22*(1), 1–8. https://doi.org/10.1002/hyp.6637

Leite-Filho, A. T., Costa, M. H., & Fu, R. (2020). The southern Amazon rainy season: The role of deforestation and its interactions with large-scale mechanisms. *International Journal of Climatology*, *40*(4), 2328–2341. https://doi.org/10.1002/joc.6335

Marengo, J. A., & Espinoza, J. C. (2016). Extreme seasonal droughts and floods in Amazonia: Causes, trends and impacts. *International Journal of Climatology*, *36*(3), 3–1050. https://doi.org/10.1002/joc.4420

McGregor, S., Timmermann, A., Stuecker, M. F., England, M. H., Merrifield, M., Jin, F.-F., & Chikamoto, Y. (2014). Recent Walker circulation strengthening and Pacific cooling amplified by Atlantic warming. *Nature Climate Change*, *4*(10), 888–892. https://doi.org/10.1038/nclimate2330

Nobre, A. D. (2014). *The future climate of Amazonia: Scientific assessment report*. CCST-INPE. 42.

Olive, D. J. (2007). Prediction intervals for regression models. *Computational Statistics & Data Analysis*, *2007*(51), 3115–3122. https://doi.org/10.1016/j.csda.2006.02.006

Ortega-Rodriguez, D. R., Sánchez-Salguero, R., Hevia, A., Granato-Souza, D., Cintra, B. B. L., Hornink, B., et al. (2023). Climate variability of the southern Amazon inferred by a multi-proxy tree-ring approach using *Cedrela fissilis* Vell. *Science of the Total Environment*, *871*. https://doi.org/10.1016/j.scitotenv.2023.162064

Percival, D. B., & Constantine, W. L. B. (2006). Exact simulation of Gaussian time series from nonparametric spectral estimates with application to bootstrapping. *Statistics and Computing*, *16*(1), 25–35. https://doi.org/10.1007/s11222-006-5198-0

Quiroz, R. S. (1983). The climate of the "El Nino" winter of 1982–83, a season of extraordinary climatic anomalies. *Monthly Weather Review*, *111*(8), 1685–1706. https://doi.org/10.1175/1520-0493(1983)111<1685:tcotnw>2.0.co;2

Rayner, N. A., Parker, D. E., Horton, E. B., Folland, C. K., Alexander, L. V., Rowell, D. P., et al. (2003). Global analyses of sea surface temperature, sea ice, and night marine air temperature since the late nineteenth century. *Journal of Geophysical Research. Atmosphere*, *108*(D14), 4407. https://doi.org/10.1029/2002JD002670

Risi, C., Bony, S., & Vimeux, F. (2008). Influence of convective processes on the isotopic composition ($\delta^{18}O$ and δD) of precipitation and water vapor in the tropics: 2. Physical interpretation of the amount effect. *Journal of Geophysical Research*, *113*(D19), D19306. https://doi.org/10.1029/2008JD009943

Ritchie, P. D., Parry, I., Clarke, J. J., Huntingford, C., & Cox, P. M. (2022). Increases in the temperature seasonal cycle indicates long-term drying trends in Amazonia. *Communications Earth & Environment*, *3*(1), 199. https://doi.org/10.1038/s43247-022-00528-0

Rodriguez-Caton, M., Morales, M. S., Rao, M. P., Nixon, T., Vuille, M., Rivera, et al. (2024). A 300-year tree-ring $\delta^{18}O$-based precipitation reconstruction for the South American Altiplano highlights decadal hydroclimate teleconnections. *Communications Earth & Environment*, *5*(1), 1–13. https://doi.org/10.1038/s43247-024-01385-9

Ronchail, J., Cochonneau, G., Molinier, M., Guyot, J.-L., De Miranda Chaves, A. G., Guimarães, V., & de Oliveira, E. (2002). Interannual rainfall variability in the Amazon basin and sea-surface temperatures in the equatorial Pacific and the tropical Atlantic Oceans. *International Journal of Climatology*, *22*(13), 1663–1686. https://doi.org/10.1002/joc.815

Rozanski, K., Araguás-Araguás, L., & Gonfiantini, R. (2013). Isotopic patterns in modern global precipitation. In P. K. Swart, K. C. Lohmann, J. Mckenzie, & S. Savin (Eds.), *Geophysical monograph series* (pp. 1–36). American Geophysical Union. https://doi.org/10.1029/GM078p0001

Salati, E., Dall'Olio, A., Matsui, E., & Gat, J. R. (1979). Recycling of water in the Amazon Basin: An isotopic study. *Water Resources Research*, *15*(5), 1250–1258. https://doi.org/10.1029/WR015i005p01250

Seber, A., & Lee, J. (2003). *Linear regression analysis*. Wiley.

Spracklen, D. V., & Garcia-Carreras, L. (2015). The impact of Amazonian deforestation on Amazon basin rainfall. *Geophysical Research Letters*, *42*(21), 9546–9552. https://doi.org/10.1002/2015GL066063

Stahle, D. W., Torbenson, M. C. A., Howard, I. M., Granato-Souza, D., Barbosa, A. C., Feng, S., et al. (2020). Pan American interactions of Amazon precipitation, streamflow, and tree growth extremes. *Environmental Research Letters*, *15*(10), 104092. https://doi.org/10.1088/1748-9326/ababc6

Sternberg, H. O. (1987). Aggravation of floods in the Amazon River as a consequence of deforestation? *Geografiska Annaler*, *69*(1), 201–219. https://doi.org/10.1080/04353676.1987.11880208

St. George, S., & Ault, T. R. (2011). Is energetic decadal variability a stable feature of the central Pacific coast's winter climate? *Journal of Geophysical Research. Atmosphere*, *116*(D12), D12102. https://doi.org/10.1029/2010JD015325

Torbenson, M. C. A., Stahle, D. W., Howard, I. M., Burnette, D. J., Villanueva-Diaz, J., Cook, E. R., & Griffin, D. (2019). Multidecadal modulation of the ENSO teleconnection to precipitation and tree growth over subtropical North America. *Paleoceanography and Paleoclimatology*, *34*(5), 886–900. https://doi.org/10.1029/2018PA003510

Trouet, V., & Oldenborgh, G. J. V. (2013). KNMI climate explorer: A web-based research tool for high-resolution paleoclimatology. *Tree-Ring Research*, *69*(1), 3–13. https://doi.org/10.3959/1536-1098-69.1.3

Vargas, D., Pucha-Cofrep, D., Serrano-Vincenti, S., Burneo, A., Carlosama, L., Herrera, M., et al. (2022). ITCZ precipitation and cloud cover excursions control *Cedrela nebulosa* tree-ring oxygen and carbon isotopes in the northwestern Amazon. *Global and Planetary Change*, *211*. https://doi.org/10.1016/j.gloplacha.2022.103791

Vinod, H. D. (2006). Maximum entropy ensembles for time series inference in economics. *Journal of Asian Economics*, *17*(6), 955–978. https://doi.org/10.1016/j.asieco.2006.09.001

Vuille, M., Bradley, R. S., Werner, M., Healy, R., & Keimig, F. (2003). Modeling $\delta^{18}O$ in precipitation over the tropical Americas: 1. Interannual variability and climatic controls. *Journal of Geophysical Research*, *108*(D6). https://doi.org/10.1029/2001JD002038

Wieloch, T., Helle, G., Heinrich, I., Voigt, M., & Schyma, P. (2011). A novel device for batch-wise isolation of α-cellulose from small-amount Wholewood samples. *Dendrochronologia*, *29*(2), 115–117. https://doi.org/10.1016/j.dendro.2010.08.008

Wigley, T. M. L., Briffa, K. R., & Jones, P. D. (1984). On the average value of correlated time series, with applications in dendroclimatology and hydrometeorology. *Journal of Applied Meteorology and Climatology*, *23*(2), 201–213. https://doi.org/10.1175/1520-0450(1984)023<0201:OTAVOC>2.0.CO;2

Wolter, K., & Timlin, M. S. (2011). El Nino/southern Oscillation behaviour since 1871 as diagnosed in an extended Multivariate ENSO Index (MEI.ext). *International Journal of Climatology*, *31*(7), 1074–1087. https://doi.org/10.1002/joc.2336

Xu, X., Zhang, X., Riley, W. J., Xue, Y., Nobre, C. A., Lovejoy, T. E., & Jia, G. (2022). Deforestation triggering irreversible transition in Amazon hydrological cycle. *Environmental Research Letters*, *17*(3). https://doi.org/10.1088/1748-9326/ac4c1d

Zapata-Ríos, G., Andreazzi, C. S., Carnaval, A. C., Rodrigues Da Costa Doria, C., Duponchelle, F., Flecker, A., et al. (2021). *Amazon assessment report 2021*. (1st ed.). UN Sustainable Development Solutions Network (SDSN). https://doi.org/10.55161/DGNM5984